Evidence of hydrocarbon nanodrops in highly ordered stratum corneum model membranes[S]

Adrian Paz Ramos,* Gert Gooris,† Joke Bouwstra,† and Michel Lafleur[1,*]

Department of Chemistry,* Université de Montréal, Montréal, Québec H3C 3J7, Canada; and Department of Drug Delivery Technology,† Leiden Academic Centre for Drug Research, 2333 CC Leiden, The Netherlands

ORCID ID: 0000-0003-3868-9803 (M.L.)

Abstract The stratum corneum (SC), the top layer of skin, dictates the rate of both water loss through the skin and absorption of exogenous molecules into the body. The crystalline organization of the lipids in the SC is believed to be a key feature associated with the very limited permeability of the skin. In this work, we characterized the organization of SC lipid models that include, as in native SC, cholesterol, a series of FFAs (saturated with C16-C24 chains), as well as a ceramide bearing an oleate chain-linked to a very long saturated acyl chain [*N*-melissoyl-oleoyloxy hexacosanoyl-D-*erythro*-sphingosine (Cer EOS)]. The latter is reported to be essential for the native SC lipid organization. Our ^{2}H-NMR, infrared, and Raman spectroscopy data reveal that Cer EOS leads to the formation of highly disordered liquid domains in a solid/crystalline matrix. The lipid organization imposes steric constraint on Cer EOS oleate chains in such a way that these hydrocarbon nanodroplets remain in the liquid state down to −30°C. These findings modify the structural description of the SC substantially and propose a novel role of Cer EOS, as this lipid is a strong modulator of SC solid/liquid balance.—Paz Ramos, A., G. Gooris, J. Bouwstra, and M. Lafleur. **Evidence of hydrocarbon nanodrops in highly ordered stratum corneum model membranes. *J. Lipid Res.* 2018.** 59: **137–143.**

Supplementary key words ceramide • ^{2}H-nuclear magnetic resonance • IR spectroscopy • phase behavior • lipids • skin

The mammalian skin barrier is a vital component of our body, tightly regulating the loss of water and the adsorption of exogenous molecules. The stratum corneum (SC), the top layer of skin, is the most important element ensuring skin impermeability. It is formed by hydrophobic protein blocks glued together with stacks of unusual lipids. The SC lipid fraction is mainly responsible for skin impermeability. As an illustration, skin becomes 20–50 times more permeable when the lipid fraction is extracted with an organic solvent (1). At this point, the origin of skin impermeability is mainly associated with the presence of lipid crystalline phases. At physiological temperature, SC lipids are mainly in a crystalline state, forming solid orthorhombic structures, which is proposed to be highly impermeable (2–4).

SC lipid composition is rather unique for biological membranes: an equimolar mixture of ceramides, FFAs, and cholesterol (Chol). There are at least 15 subclasses of ceramides in human SC, including ceramides NS, which are ceramides bearing a nonhydroxylated chain and a sphingosine base (5). Ceramides NS present different acyl chain lengths, usually from 16 to 30 carbon (C) atoms, the most abundant being the C24 chain (6, 7). Ceramide EOS, an esterified ω-hydroxy acid sphingosine, is constituted by a sphingosine base bearing a very long omega-hydroxy fatty acid with a chain length distribution between 26 C and 36 C atoms to which an unsaturated C18 fatty acid chain is esterified. There is also a chain length distribution of the FFA component, the most abundant being saturated with 22 C, 24 C, and 26 C atoms (8).

X-ray and neutron diffraction studies have shown that SC lipids form two coexisting lamellar phases with different spacing: the short periodicity phase (SPP), with a repeat distance of approximately 6 nm, and the long periodicity phase (LPP), with a periodicity of around 13 nm (9). The LPP plays an important role in the skin barrier; for example, the diffusion rate of an aminobenzoic acid derivative in model membranes lacking ceramide EOS that only form the SPP was increased compared with that in the presence of ceramide EOS that forms the LPP and SPP (10). Furthermore, ceramide EOS seems to play a crucial role in the

This work was supported by the Natural Sciences and Engineering Research Council of Canada and the Fonds Québécois de la Recherche sur la Nature et les Technologies (FQRNT) through its financial support to the Center for Self-Assembled Chemical Structures (CSACS). Additional support was provided by a Doctoral Research Scholarship for Foreign Students to A.P.R. by Fonds Québécois de la Recherche sur la Nature et les Technologies.

Manuscript received 11 September 2017 and in revised form 26 October 2017.

Published, JLR Papers in Press, November 1, 2017
DOI https://doi.org/10.1194/jlr.M080432

Abbreviations: Cer EOS, *N*-melissoyl-oleoyloxy hexacosanoyl-D-*erythro*-sphingosine; Cer NS, *N*-lignoceryl-D-*erythro*-sphingosine; Chol, cholesterol; IR, infrared; l_o, liquid-ordered phase; LPP, long periodicity phase; SC, stratum corneum; SPP, short periodicity phase.

[1]To whom correspondence should be addressed.
e-mail: michel.lafleur@umontreal.ca

[S] The online version of this article (available at http://www.jlr.org) contains a supplement.

formation of the LPP. Previous studies show that the presence of ceramide EOS is a requirement to prepare SC model membranes with both SPP and LPP and that replacing the unsaturated C18 chain of ceramide EOS by a saturated C18 chain is detrimental for the formation of the LPP (11, 12). Furthermore, some skin diseases, like atopic dermatitis and dry skin, are characterized by a low content of ceramide EOS (13), which is thought to influence the formation of the LPP and may contribute to the reduction in skin barrier.

Several models for the organization of SC lipids into the SPP and LPP have been proposed (14–18). Recently, a model based on neutron diffraction analyses showed that ceramide NS could dictate the length of the unit cell in the SPP, sharing the unit cell space with Chol and FFA. The LPP, on the other hand, could be formed of ceramide EOS and ceramide NS, surrounded by Chol and very long chain FFAs (18).

In this work, we have characterized the chain order of different components in mirror SC model lipid mixtures forming the LPP. The mixtures included 33.3 (mol)% ceramide {13.3 (mol)% of ceramide EOS with an oleate chain [*N*-melissoyl-oleoyloxy hexacosanoyl-D-*erythro*-sphingosine (Cer EOS)] and 20.0 (mol)% of [*N*-lignoceryl-D-*erythro*-sphingosine (Cer NS)]}, 33.3 (mol)% Chol, and 33.3 (mol)% FFA [0.8 (mol)% FFA16, 1.5 (mol)% FFA18, 2.9 (mol)% FFA20, and 28.2 (mol)% FFA24] (**Fig. 1**). SC FFAs actually include FFA22; however, we used a proportion of FFA24 that represents the combined amount of FFA22 and FFA24 in SC [~85 (mol)% of the total FFA], allowing us to describe the behavior of the very long FFA chains using a single representative of this class of molecules.

For the spectroscopic analysis, mirror mixtures with the same composition, but containing one deuterated species, were prepared: deuterated Cer NS-d_{47}, deuterated Cer EOS-d_{33}, or deuterated FFA24-d_{47}. The mirror mixture with FFA24-d_{47} included hydrogenated FFA16, FFA18, and FFA20.

The chain order has been characterized using three independent complementary techniques. ^{2}H-NMR is a powerful technique in the study of SC model membranes because it provides valuable information about the chain orientational order and phase behavior of the deuterated lipid constituent (19, 20). The methylene stretching vibrations, observed in the infrared (IR) and Raman spectra, allow the characterization of the lipid chain conformational order (21–23). These approaches exploit the isotopic shift effect to provide a simultaneous and independent characterization of different components in a mixture when a species with a deuterated chain is used: the C-D symmetric stretching mode ($\nu_s CD_2$) is an intrinsic probe of the deuterated chain order, while the methylene symmetric stretching band ($\nu_s CH_2$) describes the chain order of the hydrogenated components.

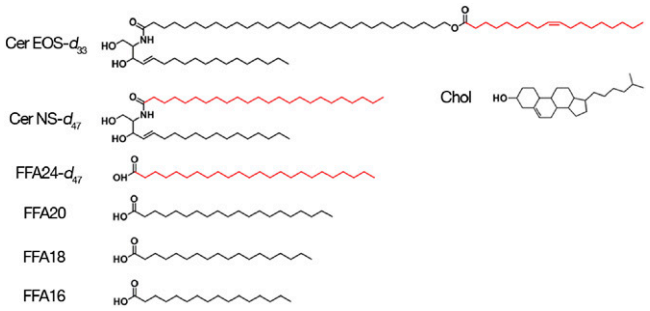

Fig. 1. The molecular structure of the lipids investigated in the present study. The deuterium-labeled portions are represented in red.

MATERIALS AND METHODS

Materials

Two ceramides, protiated Cer EOS and Cer NS, were generously provided by Evonik (Essen, Germany); their purity was >96% for Cer NS and >91% for Cer EOS. Partly deuterated Cer EOS and Cer NS (Fig. 1) (purity >99% as determined by mass spectrometry) were custom synthesized by Evonik. Palmitic acid (C16:0), stearic acid (C18:0), arachidic acid (C20:0), lignoceric acid (C24:0), and Chol, all with a purity >98%, were obtained from Sigma-Aldrich Chemie GmbH (Schnelldorf, Germany). Deuterated lignoceric acid (purity >98%) was obtained from ARC Laboratories (Apeldoorn, The Netherlands). Silicon wafers were obtained from Okmetic (Vantaa, Finland). The solvents that were used were supplied by Labscan (Dublin, Ireland) and were of analytical grade.

Sample preparation

The synthetic ceramides, Chol, and FFAs were used in an equimolar ratio. The molar ratio between Cer EOS and Cer NS was 0.4:0.6, while the fatty acids were used in a molar ratio of FFA24:FFA20:FFA18:FFA16 84.6:8.75:4.57:2.05. To prepare the mixtures, the appropriate amount of lipids (~20 mg) was dissolved in a chloroform/methanol (2:1 v/v) mixture at a concentration of 5 mg/ml. Subsequently, the lipids were sprayed on a silicon substrate on an area of 1.5 × 4.0 cm^2 using a Camag Linomat IV sample applicator (Muttenz, Switzerland). Spraying was performed at a rate of 5 μl/min under a gentle stream of nitrogen gas. Subsequently, the lipid mixture was equilibrated for 10 min at 70°C, close to the melting temperature of the lipid mixture. After equilibration, the sample was slowly cooled down and carefully scraped from the support and inserted into a NMR tube. The NMR tube was closed air tight under a flow of argon gas to prevent oxidation.

Small angle X-ray diffraction

Small angle X-ray diffraction was used to determine the lamellar organization. The small angle X-ray diffraction measurements were carried out at the European Synchrotron Radiation Facility (Grenoble, France) at station BM26B. The pattern was collected on a Pilatus 1M detector for two times 60 s. The sample-to-detector distance was approximately 2 m. The scattering intensity I (arbitrary units) was measured as a function of the scattering vector q (in nm^{-1}), defined as $q = 4\pi\sin(\theta)/\lambda$, in which θ is the scattering angle and λ is the wavelength. From the positions of the peaks, the repeat distance was calculated $d = n2\pi/q_n$, in which n is the order of the diffraction peak and q_n the peak position of the nth order.

^{2}H-NMR analysis

Solid-state NMR measurements were performed on a Bruker Avance II 400 WB spectrometer at a ^{2}H-frequency of 61.4 MHz,

using a Bruker static probe with a 5 mm coil. The spectra were acquired using a quadrupolar echo pulse sequence with a 1.80 μs 90° pulse, separated by an interpulse delay of 40 μs, and a recycle time of 50 s for slow-relaxing solid phase and 0.3 s for gel and disordered phases. Samples were placed into a Teflon holder, hydrated with an acetate buffer (50 mM, pH 5), and incubated at 37°C. After 24 h of incubation, a first spectrum was recorded. Then, samples were left at 37°C for 7 days. A second spectrum was collected after the week. In all cases, there was no difference between this spectrum and the one collected after 1 day incubation, suggesting that the sample was at thermodynamic equilibrium. A minimum of 1,000 scans was collected for each spectrum.

IR analysis

IR spectroscopy analyses were carried out using a Thermo Nicolet 4700 spectrometer. A portion of hydrated lipid mixture was put between two CaF_2 windows separated by a 5 μm-thick Teflon spacer. An additional 25 μl aliquot of acetate buffer was added to the sample to maintain hydration during the measurements. This assembly was inserted in a temperature-controlled brass sample holder and placed into the spectrometer. The spectra were acquired as a function of increasing temperature, varying from 25°C to 70°C with a temperature step of 2°C and an equilibration period of 5 min for each temperature. Spectra were recorded co-adding 32 scans with a nominal spectral resolution of 1 cm^{-1}. The reported band positions correspond to the band maximum.

Raman analysis

Raman measurements were performed using a WITec confocal Raman system, with an immersion 63× objective (NA = 1.0). A small portion of the sample was placed on a CaF_2 window and gently squeezed in order to obtain a relatively flat surface. The sample was immersed in the acetate buffer to ensure complete hydration during the measurements. The sample temperature was adjusted to 33°C. A 532 nm laser was used as excitation source with a 10 mW power at the sample surface. Spectra were recorded between 1,000 and 3,200 cm^{-1} with a spectral resolution of 1 cm^{-1}, the acquisition time for each spectrum was 3 s.

RESULTS

The X-ray diffraction curve of the protiated sample is provided in supplemental Fig. S1. The position of the peaks revealed a single lamellar phase spacing with a repeat distance of 12.4 nm, corresponding to the LPP. In addition, phase separated crystalline Chol was present.

The ^{2}H-NMR spectra of Cer EOS/Cer NS/FFA/Chol mixtures were recorded from mirror mixtures made with FFA24-d_{47}, Cer NS-d_{47}, or Cer EOS-d_{33}. **Figure 2** shows the spectra evolution of the deuterium-labeled mixtures as a function of temperature.

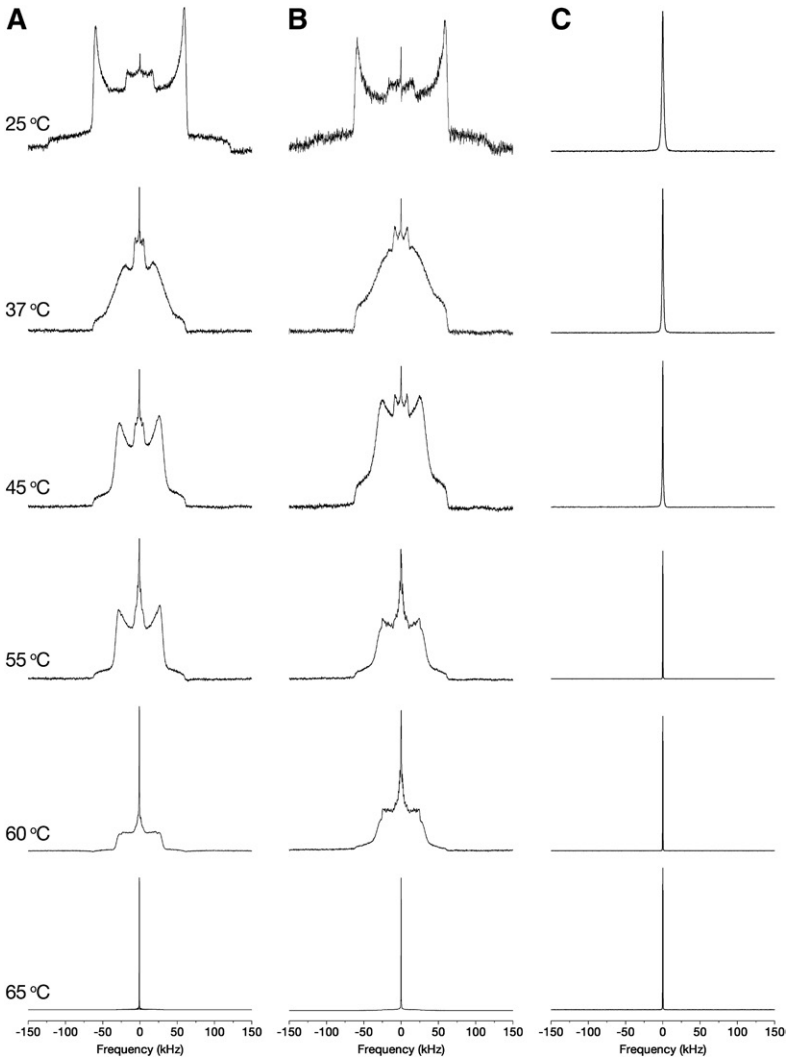

Fig. 2. Thermal evolution of the ^{2}H-NMR spectra of the Cer EOS/Cer NS/FFA/Chol mirror mixtures; FFA24-*d* (A), Cer NS-*d* (B), and Cer EOS-*d* (C). The spectra are normalized to the same height.

Figure 2A shows the behavior of deuterated lignoceric acid in the Cer EOS/Cer NS/FFA/Chol mixture. At low temperatures, the spectrum was typical of lipids in a solid phase, i.e., composed of two patterns: a broad signal with a quadrupolar splitting of ~120 kHz, which corresponds to the equivalent methylene groups along the FFA24 all-*trans* immobile (on the NMR timescale) acyl chain, and a second powder pattern, with a quadrupolar splitting of ~35 kHz due to the terminal methyl groups. The FFA24 spectrum at ~37°C, with a width at the base of ~128 kHz, indicated a transition of the fatty acid toward a gel phase. Upon heating up to 60°C, the evolution of the spectrum showed an increase of chain rotational diffusion while remaining in an almost all-*trans* configuration (2, 24). Heating above 60°C caused a transition toward a liquid-ordered phase (l_o). In this phase, FFA24 molecules underwent fast rotational motion along the lipid long axis, while the orientational order of lipid chains remained high. The spectrum shape was associated with the overlapping powder patterns due to the order gradient along the chain. Heating above 65°C caused a transition to an isotropic phase, characterized by a narrow central peak corresponding to FFA24 molecules that reoriented randomly on the NMR time scale.

The behavior of deuterated Cer NS in the mixture is described in Fig. 2B. Cer NS experienced phase transitions analogous to those of FFA24 in the mixture, i.e., solid phase at the physiological temperature of the skin, a solid-to-gel phase transition at ~37°C, a gel-to-l_o phase transition at around 60°C, and finally a transition toward an isotropic phase starting at 70°C.

The mixture containing Cer EOS with a deuterated oleate chain (Fig. 2C) showed a completely different behavior. This sample exhibited a narrow signal over all the investigated temperature range. This ^{2}H-NMR signature is typical of molecules undergoing isotropic motions, an observation suggesting that the oleate chains were highly disordered, as in a liquid phase. Four additional experiments were carried out in order to discard micelle formation and/or extended lipid separation. First, the sample was suspended in a large excess of buffer (1 ml) and centrifuged at 2,200 *g* for 30 min. The supernatant was discarded and the spectrum of the pellet was recorded: it showed only the narrow line. This result indicated that Cer EOS was not forming small aggregates that would have remained in the supernatant, but this lipid was included in the lipid matrix. Furthermore, mass spectrometry showed that Cer EOS was intact after the measurements. Second, the spectrum of the sample that was dehydrated by freeze-drying was recorded and it showed only the narrow line (see supplemental Fig. S2). This finding indicated that the driving force for the formation of a solid matrix with liquid-phase domain organization is not primarily hydrophobic interactions, as it was observed in the absence of water. Third, the dry sample was cooled down and the spectrum remained essentially a narrow line down to −20°C (supplemental Fig. S2). Fourth, a Cer EOS/Cer NS/FFA/Chol mixture sample containing both Cer EOS-d_{33} and FFA24-d_{47} was prepared. The spectrum showed the wide powder pattern of immobile deuterated chains coexisting with the narrow line (see supplemental Fig. S3), indicating the coexistence of solid and liquid-like lipids in the sample. The relative areas of these spectral components agreed with the proportion and number of deuterium nuclei of FFA24-d_{47} and Cer EOS-d_{33}, considering the former contributing only to the solid-phase signal and the latter to the narrow signal. The intensity of the narrow line remained constant up to −10°C. Upon further cooling, a pattern associated with solid phase grew and the spectrum displayed only this solid powder pattern at −50°C.

IR spectroscopy was used to probe changes in the conformational order of lipid chains because the positions of the methylene stretching vibrations are sensitive to *trans/gauche* isomerization of acyl chains (25–27). The position of the deuterated methylene symmetric stretching band (ν_sCD_2) was associated with deuterated chain order, while the position of the hydrogenated methylene symmetric stretching band (ν_sCH_2) described the overall conformational order of all the hydrogenated lipid chains in the mixture. **Figure 3** shows the evolution of these spectral parameters as a function of temperature for the Cer EOS/Cer NS/FFA/Chol mixtures.

In the sample containing FFA24-d_{47} (Fig. 3A), the position of the ν_sCD_2 band remained at ~2,088.5 cm^{-1} between 25°C and 60°C, indicating a highly ordered FFA24-d_{47} acyl chain (25, 26). Upon heating above 60°C, the band position abruptly shifted toward high wavenumbers, reaching 2,095.6 cm^{-1} at 70°C. This value is characteristic of a disordered acyl chain (28, 29) and the band shift was associated with the disordering of FFA24-d_{47} chains, as previously observed for analogous mixtures (2, 30). At low temperatures, the ν_sCH_2 band was found at around 2,850 cm^{-1}, a value indicative of high chain order (25, 26). The band position slightly increased by ~1 cm^{-1} between 30°C and 40°C, presumably due to a solid-to-gel transition, as reported previously for analogous mixtures (2, 30). Its value increased abruptly at 60°C, reaching 2,853.5 cm^{-1} at 70°C. This upshift was indicative of an increase of the conformational chain disorder (31, 32).

A similar behavior was observed for the sample containing deuterated Cer NS (Fig. 3B). The ν_sCD_2 band was observed at ~2,088.5 cm^{-1}, from 25°C to about 60°C, indicating that the Cer NS-d_{47} chain was highly ordered. Upon further heating, the band position upshifted and reached 2,094.7 cm^{-1} at 70°C, reporting the increase of conformational chain disorder of the Cer NS chain. The thermal profile obtained for the ν_sCH_2 band position was similar to that of the sample containing FFA24-d_{47}.

The mixture containing Cer EOS-d_{33} (Fig. 3C) showed high values for the position of the ν_sCD_2 band, with a mean value of 2,095.7 ± 0.8 cm^{-1} over the entire temperature range. The band position was actually very similar to those obtained for FFA24-d_{47} and Cer NS-d_{47} molecules at 70°C. These results indicated that the oleate chain of Cer EOS was highly disordered, even at low temperatures. The hydrogenated lipid acyl chains, however, followed a behavior analogous to the previous samples. The ν_sCH_2 position was ~2,849.5 cm^{-1} at 25°C, increased slightly between 32°C and 40°C, was constant from 40°C to 60°C, and rapidly increased

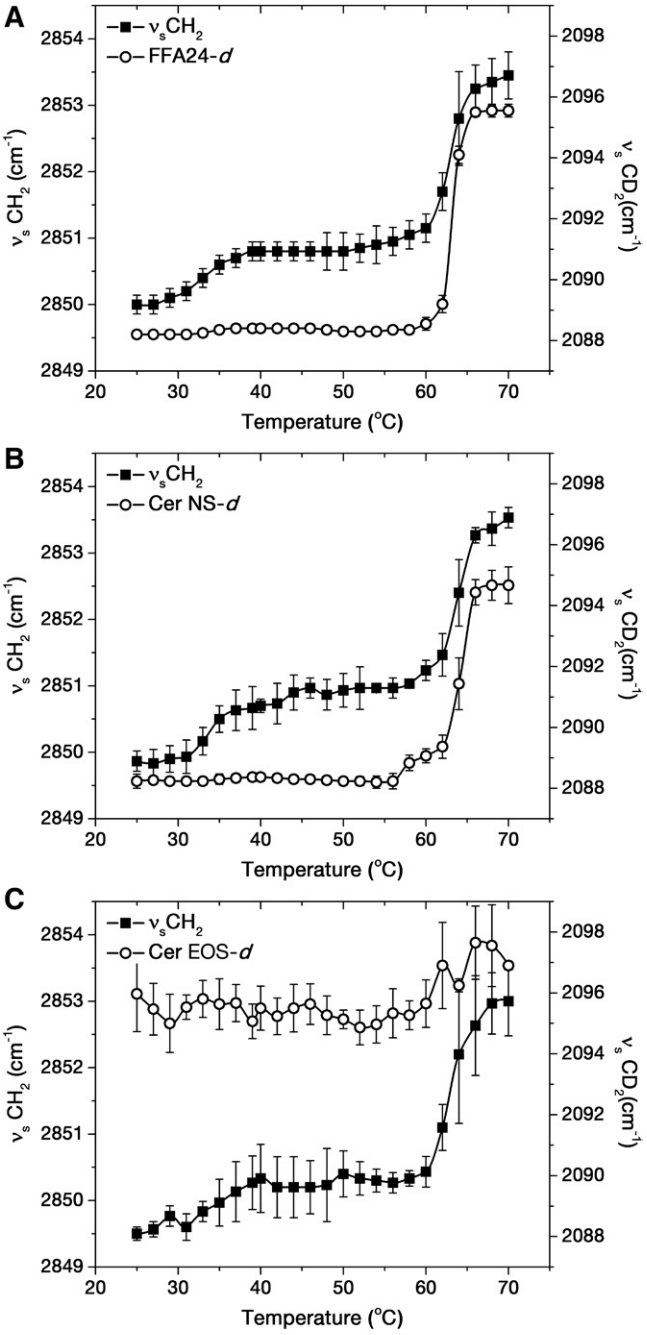

Fig. 3. Thermotropic behavior of Cer EOS/Cer NS/FFA/Chol mixtures containing FFA24-d_{47} (A), Cer NS-d_{47} (B), and Cer EOS-d_{33} (C). The data points represent the average and the standard deviation for n = 3.

to ~2,853 cm^{-1} at 70°C. It should be noted that the $\nu_s CH_2$ position was systematically slightly lower (by about 0.5 cm^{-1}) than those recorded for the mixtures with FFA24-d_{47} or Cer NS-d_{47}. In these mixtures, Cer EOS contributed to the C-H stretching region (as the hydrogenated form was present) and its high conformational disorder was likely responsible for the small upshift of the $\nu_s CH_2$ position, which described the overall order of all the hydrogenated chain species.

In order to further characterize the chain order, the C-D stretching region of the Raman spectra of the mirror mixtures was analyzed (**Fig. 4**). This region was dominated by a band at ~2,100 cm^{-1}, assigned to the symmetric C-D stretching of the CD_2 groups (29). Its width increases with the conformational disorder of the deuterated acyl chain (31). The band width at 65% of the height was 21.6 cm^{-1} for the mixture, including FFA24-d_{47} and Cer NS-d_{47}, and 42.4 cm^{-1} for that with CerEOS-d_{33}. These observations also indicated that the acyl chains of FFA24 and Cer NS were both ordered while the oleate chain in CerEOS was highly disordered, as inferred from the ^{2}H-NMR and IR spectroscopy results.

DISCUSSION

The present work reveals a novel feature of SC lipid organization: this lipid structure is formed by solid lipids in which highly disordered liquid domains formed by the oleate chain of CerEOS are embedded. The existence of a large solid/crystalline component in the SC lipid fraction is a well-established aspect: for example, wide-angle X-ray diffraction patterns reported crystalline structures in human SC (32). IR spectra of SC model mixtures, as well as real SC, showed highly ordered chains with orthorhombic packing (28, 33). Solid-state NMR of several model mixtures mimicking SC lipid phase mainly gave rise to the pattern characteristic of immobile acyl chains (20, 34). The presence of a fluid lipid fraction was proposed for the first time more than 20 years ago by Forslind (16). Under this hypothesis, crystalline domains forming mosaic-like structures were bound by lipids in a fluid phase. This model rationalized the low permeability of SC, as well as its flexibility (16). A detailed NMR study supported this model and indicated that a small fraction of lipids in intact SC was mobile (35). Recently, an organization of SC lipids reproducing the SPP and LPP structure based on neutron diffraction results was proposed (18). This model presents the possible arrangement of the various lipid components in the LPP stacked layers (**Fig. 5**). The proposed lipid arrangement leaves a

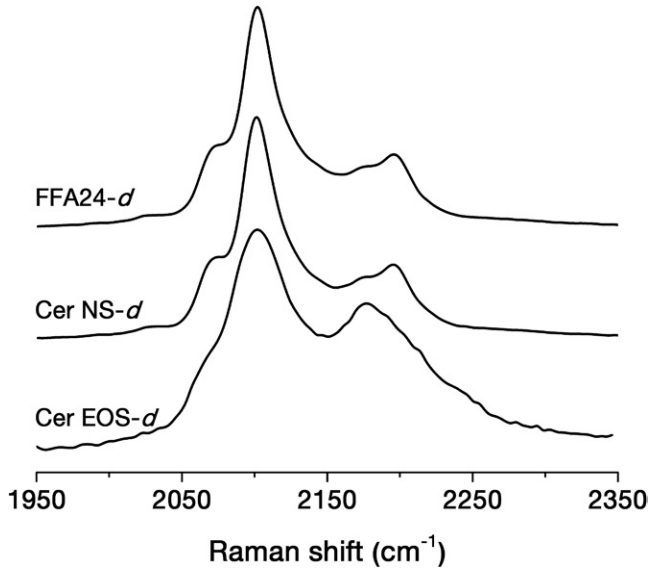

Fig. 4. The C-D stretching region of the Raman spectra for the Cer EOS/Cer NS/FFA/Chol mirror mixtures.

JOURNAL OF LIPID RESEARCH ASBMB

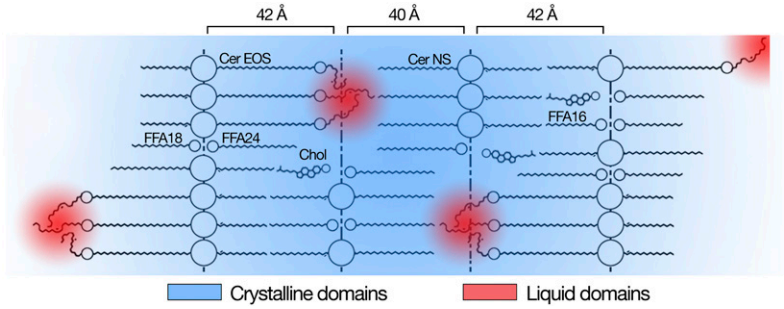

Fig. 5. Suggested locations of the liquid domains into the crystalline lipid matrix. Polar head groups and ester bonds are represented by circles.

limited space for the linoleate chain of Cer EOS and it was proposed that the chain, in contrast to the fully extended acyl chains of the other lipid species, would be highly disordered. These disordered chains could not be observed in the diffraction experiments. However, it was shown by IR spectroscopy that the deuterated linoleate chain of Cer EOS in a model mixture similar to the one used in the present work and forming exclusively LPP was fluid (36). The present results reveal that the unsaturated chain of Cer EOS experiences liquid-like dynamics, proposing the existence of hydrocarbon droplets in the SC solid lipid matrix. It has been shown (37) that the model mixtures including oleate or linoleate as the unsaturated chain of Cer EOS behaved similarly, as they both formed the LPP, and their unsaturated chains were proposed to be disordered by IR spectroscopy. It should be pointed out that, in the present work, the liquid domains were observed even in the absence of water. This observation is actually consistent with previous results obtained on intact SC showing that the small fraction of mobile lipids was still observed with completely dry SC (35). The unexpected presence of liquid domains is proposed to be associated with the steric confinement of the oleate chains. The crystallization process leads to the ordering of all the methylene segments into an all-*trans* configuration to maximize interchain van der Waals interactions. According to the proposed lipid organization, the dimension of the space available to the oleate chain is too short for a fully extended oleate chain (~19 Å) (38). This confinement would prevent chain stretching and lipid solidification. The fact that the oleate chain of Cer EOS remained in the liquid state at a temperature as low as −20°C, as observed by ^{2}H-NMR, is an exceptional behavior, as compounds bearing an oleate chain have a melting point considerably higher than this value. The melting point of oleic acid is 16.3°C (39). The melting point of *cis*-9-octadecen-1-ol is between 0°C and 3°C (39), that of *cis*-9-octadecenylamine is 25°C (39), that of *cis*-9-octadecenoamide is 76°C (39), and that of *cis*-9-octadecene is 0–2°C (40). The depression of this melting point is reminiscent of the decrease in the crystallization temperature of molecules trapped in nanopores [for reviews, see (41, 42)]. Such a phenomenon is even observed with water when the geometrical constraints associated with the pore size hinder the formation of the tetrahedral ice structure by the water molecules (43).

The dynamics of the oleate chain remained, even at −20°C, fast on the NMR time scale (10^{-5} s) as the quadrupolar interactions were completely averaged out. The liquid-like behavior of the oleate chains suggests that they are not isolated from each other, but a certain number of them are grouped together, forming local hydrocarbon nanodroplets (Fig. 5). The presence of an unsaturation in the chain is a structural element favoring the formation of a liquid phase and increasing chain disorder (44); for example, the melting points of oleic acid and octadecanoic acid are 14°C and 69°C, respectively (39). Interestingly, the presence of an unsaturation in the ester-linked acyl chain of Cer EOS appears to be essential for the formation of the LPP: small angle X-ray observations of mixtures made with human ceramide/Cer EOS/FFAs/Chol showed the formation of the LPP when Cer EOS bore an unsaturated linoleate or oleate chain, but not a stearate (saturated) chain (12, 37). In these mixtures, the hydrocarbon chain of Cer EOS was more disordered when it was a linoleate or oleate chain than when it was a saturated stearate chain, reinforcing the conclusion that a distinct structure that includes liquid domains is formed with Cer EOS bearing an unsaturated chain.

The existence of liquid domains in the SC matrix could lead to revising the understanding of skin barrier property. It has been proposed that the presence of small solid/crystalline domains in the SC lipid fraction would make the diffusion path extremely tortuous, leading to a very limited permeability (45). The presence of liquid hydrocarbon droplets in the matrix could actually be a key element contributing to the SC impermeability. These apolar domains located in the head group regions would act as obstacles for the diffusion of hydrophilic compounds through the SC. Moreover, they could act as traps for the apolar species, which would strongly partition in these hydrocarbon liquid droplets. The migration of the SC matrix toward the surface and the subsequent shedding would be an efficient way to prevent the penetration of apolar compounds in the body. This hypothesis is supported by the permeability measurements showing that a SC model mixture lacking Cer EOS, and therefore not forming the characteristic LPP, displayed a 2-fold increased permeability compared with the corresponding model mixture that included Cer EOS, which forms the LPP (10). The putative role of these liquid domains in SC impermeability provides a structural rationale for the phenomenological link between the presence of the LPP and the skin barrier impermeability.

The authors would like to thank Evonik (Essen, Germany) for their generous provision of CERs and the personnel at the DUBBLE beam line 26b at the European Synchrotron Radiation Facility located at Grenoble, France for their assistance during the X-ray diffraction measurements.

REFERENCES

1. Blank, I. H. 1952. Factors which influence the water content of the stratum corneum. *J. Invest. Dermatol.* **18:** 433–440.
2. Ramos, A. P., and M. Lafleur. 2015. Chain length of free fatty acids influences the phase behavior of stratum corneum model membranes. *Langmuir.* **31:** 11621–11629.
3. Stahlberg, S., B. Školová, P. K. Madhu, A. Vogel, K. Vávrová, and D. Huster. 2015. Probing the role of the ceramide acyl chain length and sphingosine unsaturation in model skin barrier lipid mixtures by ^{2}H solid-state NMR spectroscopy. *Langmuir.* **31:** 4906–4915.
4. Pham, Q. D., D. Topgaard, and E. Sparr. 2017. Tracking solvents in the skin through atomically resolved measurements of molecular mobility in intact stratum corneum. *Proc. Natl. Acad. Sci. USA.* **114:** E112–E121.
5. van Smeden, J., W. A. Boiten, T. Hankemeier, R. Rissmann, J. A. Bouwstra, and R. J. Vreeken. 2014. Combined LC/MS-platform for analysis of all major stratum corneum lipids, and the profiling of skin substitutes. *Biochim. Biophys. Acta.* **1841:** 70–79.
6. Bouwstra, J. A., G. S. Gooris, K. Cheng, A. Weerheim, W. Bras, and M. Ponec. 1996. Phase behavior of isolated skin lipids. *J. Lipid Res.* **37:** 999–1011.
7. t'Kindt, R., L. Jorge, E. Dumont, P. Couturon, F. David, P. Sandra, and K. Sandra. 2012. Profiling and characterizing skin ceramides using reversed-phase liquid chromatography-quadrupole time-of-flight mass spectrometry. *Anal. Chem.* **84:** 403–411.
8. Norlén, L., I. Nicander, A. Lundsjö, T. Cronholm, and B. Forslind. 1998. A new HPLC-based method for the quantitative analysis of inner stratum corneum lipids with special reference to the free fatty acid fraction. *Arch. Dermatol. Res.* **290:** 508–516.
9. Mojumdar, E. H., G. S. Gooris, D. J. Barlow, M. J. Lawrence, B. Deme, and J. A. Bouwstra. 2015. Skin lipids: localization of ceramide and fatty acid in the unit cell of the long periodicity phase. *Biophys. J.* **108:** 2670–2679.
10. de Jager, M., W. Groenink, R. Bielsa i Guivernau, E. Andersson, N. Angelova, M. Ponec, and J. Bouwstra. 2006. A novel in vitro percutaneous penetration model: evaluation of barrier properties with p-aminobenzoic acid and two of its derivatives. *Pharm. Res.* **23:** 951–960.
11. de Jager, M. W., G. S. Gooris, I. P. Dolbnya, W. Bras, M. Ponec, and J. A. Bouwstra. 2004. Novel lipid mixtures based on synthetic ceramides reproduce the unique stratum corneum lipid organization. *J. Lipid Res.* **45:** 923–932.
12. Bouwstra, J. A., G. S. Gooris, F. E. R. Dubbelaar, and M. Ponec. 2002. Phase behavior of stratum corneum lipid mixtures based on human ceramides: the role of natural and synthetic ceramide 1. *J. Invest. Dermatol.* **118:** 606–617.
13. Imokawa, G., A. Abe, K. Jin, Y. Higaki, M. Kawashima, and A. Hidano. 1991. Decreased level of ceramides in stratum corneum of atopic dermatitis: an etiologic factor in atopic dry skin? *J. Invest. Dermatol.* **96:** 523–526.
14. Boncheva, M. 2014. The physical chemistry of the stratum corneum lipids. *Int. J. Cosmet. Sci.* **36:** 505–515.
15. Kessner, D., M. Kiselev, S. Dante, T. Hauss, P. Lersch, S. Wartewig, and R. H. Neubert. 2008. Arrangement of ceramide [EOS] in a stratum corneum lipid model matrix: new aspects revealed by neutron diffraction studies. *Eur. Biophys. J.* **37:** 989–999.
16. Forslind, B. 1994. A domain mosaic model of the skin barrier. *Acta Derm. Venereol.* **74:** 1–6.
17. Norlén, L. 2001. Skin barrier structure and function: the single gel phase model. *J. Invest. Dermatol.* **117:** 830–836.
18. Mojumdar, E. H., G. S. Gooris, D. Groen, D. J. Barlow, M. J. Lawrence, B. Demé, and J. A. Bouwstra. 2016. Stratum corneum lipid matrix: location of acyl ceramide and cholesterol in the unit cell of the long periodicity phase. *Biochim. Biophys. Acta.* **1858:** 1926–1934.
19. Davis, J. H. 1983. The description of membrane lipid conformation, order and dynamics by ^{2}H-NMR. *Biochim. Biophys. Acta.* **737:** 117–171.
20. Fenske, D. B., J. L. Thewalt, M. Bloom, and N. Kitson. 1994. Models of stratum corneum intercellular membranes: ^{2}H NMR of macroscopically oriented multilayers. *Biophys. J.* **67:** 1562–1573.
21. Wunder, S. L., and S. D. Merajver. 1981. Raman spectroscopic study of the conformational order in hexadecane solutions. *J. Chem. Phys.* **74:** 5341–5346.
22. Moore, D. J., M. E. Rerek, and R. Mendelsohn. 1997. FTIR spectroscopy studies of the conformational order and phase behavior of ceramides. *J. Phys. Chem. B.* **101:** 8933–8940.
23. Snyder, R. G., S. L. Hsu, and S. Krimm. 1978. Vibrational spectra in the C-H stretching region and the structure of the polymethylene chain. *Spectrochim. Acta.* **34:** 395–406.
24. Jansson, M., R. L. Thurmond, J. A. Barry, and M. F. Brown. 1992. Deuterium NMR study of intermolecular interactions in lamellar phases containing palmitoyllysophosphatidylcholine. *J. Phys. Chem.* **96:** 9532–9544.
25. Mendelsohn, R., C. R. Flach, and D. J. Moore. 2006. Determination of molecular conformation and permeation in skin via IR spectroscopy, microscopy, and imaging. *Biochim. Biophys. Acta.* **1758:** 923–933.
26. Mendelsohn, R., and D. J. Moore. 1998. Vibrational spectroscopic studies of lipid domains in biomembranes and model systems. *Chem. Phys. Lipids.* **96:** 141–157.
27. Gooris, G. S., and J. A. Bouwstra. 2007. Infrared spectroscopic study of stratum corneum model membranes prepared from human ceramides, cholesterol, and fatty acids. *Biophys. J.* **92:** 2785–2795.
28. Moore, D. J., M. E. Rerek, and R. Mendelsohn. 1997. Lipid domains and orthorhombic phases in model stratum corneum: evidence from Fourier transform infrared spectroscopy studies. *Biochem. Biophys. Res. Commun.* **231:** 797–801.
29. Mendelsohn, R., S. Sunder, and H. J. Bernstein. 1976. Deuterated fatty acids as Raman spectroscopic probes of membrane structure. *Biochim. Biophys. Acta.* **443:** 613–617.
30. Oguri, M., G. S. Gooris, K. Bito, and J. A. Bouwstra. 2014. The effect of the chain length distribution of free fatty acids on the mixing properties of stratum corneum model membranes. *Biochim. Biophys. Acta.* **1838:** 1851–1861.
31. Mendelsohn, R., and C. C. Koch. 1980. Deuterated phospholipids as Raman spectroscopic probes of membrane structure. *Biochim. Biophys. Acta.* **598:** 260–271.
32. Bouwstra, J. A., G. S. Gooris, J. A. van der Spek, and W. Bras. 1991. Structural investigations of human stratum corneum by small-angle X-ray scattering. *J. Invest. Dermatol.* **97:** 1005–1012.
33. Moore, D. J., R. G. Snyder, M. E. Rerek, and R. Mendelsohn. 2006. Kinetics of membrane raft formation: fatty acid domains in stratum corneum lipid models. *J. Phys. Chem. B.* **110:** 2378–2386.
34. Brief, E., S. Kwak, J. T. J. Cheng, N. Kitson, J. Thewalt, and M. Lafleur. 2009. Phase behavior of an equimolar mixture of N-palmitoyl-d-erythro-sphingosine, cholesterol, and palmitic acid, a mixture with optimized hydrophobic matching. *Langmuir.* **25:** 7523–7532.
35. Björklund, S., A. Nowacka, J. A. Bouwstra, E. Sparr, and D. Topgaard. 2013. Characterization of stratum corneum molecular dynamics by natural-abundance (13)C solid-state NMR. *PLoS One.* **8:** e61889.
36. Janssens, M., G. S. Gooris, and J. A. Bouwstra. 2009. Infrared spectroscopy studies of mixtures prepared with synthetic ceramides varying in head group architecture: coexistence of liquid and crystalline phases. *Biochim. Biophys. Acta.* **1788:** 732–742.
37. de Sousa Neto, D., G. Gooris, and J. Bouwstra. 2011. Effect of the ω-acylceramides on the lipid organization of stratum corneum model membranes evaluated by X-ray diffraction and FTIR studies (Part I). *Chem. Phys. Lipids.* **164:** 184–195.
38. Abrahamsson, S., and I. Ryderstedt-Nahringbauer. 1962. The crystal structure of the low-melting form of oleic acid. *Acta Crystallogr.* **15:** 1261–1268.
39. Haynes, W. M. editor. 2016. CRC Handbook of Chemistry and Physics. 97th edition. CRC Press, Boca Raton, FL.
40. Deatherage, F. E., and H. S. Olcott. 1939. Synthesis of cis-9-octadecene, 9-octadecyne and 9,10-octadecane-diol. *J. Am. Chem. Soc.* **61:** 630–631.
41. Mataz, A., and B. M. Gregory. 2005. Effects of confinement on material behaviour at the nanometre size scale. *J. Phys. Condens. Matter.* **17:** R461–R524.
42. Jiang, Q., and M. D. Ward. 2014. Crystallization under nanoscale confinement. *Chem. Soc. Rev.* **43:** 2066–2079.
43. Cerveny, S., F. Mallamace, J. Swenson, M. Vogel, and L. Xu. 2016. Confined water as model of supercooled water. *Chem. Rev.* **116:** 7608–7625.
44. Seelig, A., and J. Seelig. 1977. Effect of a single cis double bond on the structure of a phospholipid bilayer. *Biochemistry.* **16:** 45–50.
45. Menon, G. K., G. W. Cleary, and M. E. Lane. 2012. The structure and function of the stratum corneum. *Int. J. Pharm.* **435:** 3–9.